Adsorption and Reaction of Methanol Molecule on Nickel Cluster Ions, Ni_n^+ ($n = 3-11$)

Masahiko Ichihashi,[†] Tetsu Hanmura,[‡] Ramkuber T. Yadav,[‡] and Tamotsu Kondow*[,†]

Cluster Research Laboratory, Toyota Technological Institute: in East Tokyo Laboratory, Genesis Research Institute, Inc., 717-86 Futamata, Ichikawa, Chiba 272-0001, Japan, and East Tokyo Laboratory, Genesis Research Institute, Inc., 717-86 Futamata, Ichikawa, Chiba 272-0001, Japan

Received: August 8, 2000; In Final Form: September 26, 2000

The reactions of methanol on a size-selected nickel cluster ion, Ni_n^+ ($n = 3-11$), were investigated at collision energies less than 1.0 eV in a beam-gas geometry. Dominant reactions were methanol chemisorption, demethanation, and carbide formation. The absolute cross sections of these different reactions were measured and found to change dramatically with the cluster size; the demethanation proceeds preferentially on Ni_4^+, the carbide formation on $Ni_{7,8}^+$, and the chemisorption on Ni_6^+. A kinematic model explains the size-dependent characteristics that the chemisorption proceeds efficiently if the barrier height between the physisorbed and the chemisorbed states is low, and the demethanation and the carbide formation proceed otherwise. The rate of the carbide formation depends sensitively on an Ni−Ni distance of Ni_n^+ so that it proceeds only on $Ni_{7,8}^+$.

1. Introduction

Reactivity of nickel cluster ions, Ni_n^+, has been investigated with particular attention to their size-dependent reactivity, because nickel is one of the most important and frequently used elements in practical catalysis, in which the size distribution of nickel aggregates is closely related to their reactivity and selectivity. In this connection, several studies have been reported so far.[1−6] For instance, Irion and co-workers have investigated dehydrogenation of ethylene on Ni_n^+ ($n = 2-15$) and revealed that Ni_n^+ with $n = 2$, 5−15 reacts with ethylene to form $Ni_n^+(C_2H_2)_m$, whereas $Ni_{3,4}^+$ is nonreactive. Their measurements have been performed in an ion cyclotron resonance cavity, so that Ni_n^+ collides with ethylene many times.[1] Similar size-specific reactions between Ni_n^+ ($n = 4-31$) and CO have been reported by Wöste and his collaborators;[4,5] $Ni_n(CO)_i^+$ is produced in the entire n-range studied, while $Ni_mC(CO)_p^+$ only from $Ni_{4,5,7}^+$. The studies of this kind have been undertaken more or less under multiple collision conditions, which introduces undesired complexity in understanding the reaction mechanism.

To elucidate the size-specific reactivity, we have investigated reactions of methanol on size- and energy-selected nickel cluster ions, Ni_n^+ ($n = 3-11$), under single collision conditions. Methanol was chosen as the reactant in the present study, because methanol is one of the basic chemicals and often emerges as a reaction intermediate and a precursor in synthesis, decomposition, and oxidation reactions involving hydrocarbons, such as the Fischer−Tropsch process. Reactions between methanol and various metal clusters have been investigated by use of infrared photodissociation spectroscopy[7−13] and by Car−Parrinello calculation.[13,14]

2. Experimental Section

A part of the apparatus employed in the present study has been reported in our previous papers,[15−18] so that only the equipment used in the present experiment is described in detail. As shown in Figure 1, a xenon-ion beam was produced from an ion source (CORDIS Ar25/35c, Rokion Ionenstahl-Technologie), accelerated to 10 keV, and divided into four beams by a series of acceleration plates. Each Xe^+ beam was collimated by water-cooled 30-mm long tubes of 9 mm in diameter and was allowed to bombard one of four different nickel targets (Nilaco, 99.7%) cooled by water. The ions sputtered from the targets were focused by conically shaped electrodes into the first octopole ion guide (OPIG) with an opening of 18 mm in diameter. The ions were decelerated in the OPIG and cooled in helium gas ($\approx 10^{-3}$ Torr) at a temperature of 77−300 K. Impurities in the helium gas were removed by passing through a tube in a form of a helical coil, which was immersed in liquid nitrogen. The cluster ions thus cooled were transported in the second and the third OPIG's and mass-selected in the first quadrupole mass filter (Extrel, 162-8). A size-selected cluster ion was admitted into a collision region in the fourth OPIG surrounded by a reaction cell filled with methanol gas at a pressure of $\approx 5 \times 10^{-5}$ Torr. The pressure in the reaction cell was measured by a spinning rotor gauge (MKS, SRG-2). Product ions in the collision region transported through the fourth OPIG were mass-analyzed in the second quadrupole mass filter (Extrel, 162-8) and were detected by an ion-conversion dynode biased

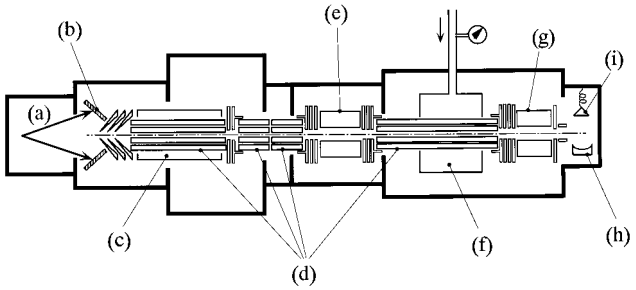

Figure 1. Schematic drawing of the apparatus used. (a) Xenon ion beam, (b) nickel target, (c) helium gas, (d) octopole ion beam guide (OPIG), (e) first quadrupole mass filter, (f) collision chamber filled with methanol gas, (g) second quadrupole mass filter, (h) ion-conversion dynode, and (i) secondary electron multiplier.

[†] Cluster Research Laboratory, Toyota Technological Institute: in East Tokyo Laboratory.
[‡] East Tokyo Laboratory.

10.1021/jp0028610 CCC: $19.00
Published on Web 12/01/2000

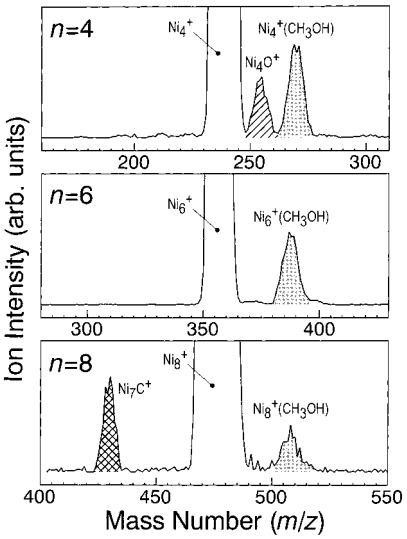

Figure 2. Mass spectra of ions produced in the collision of Ni_n^+ (n = 4, 6, and 8) with CH_3OH at a collision energy of 0.2 eV and at an internal temperature of 300 K (see text for the definition of the internal temperature).

by −10 kV, which was followed with a secondary electron multiplier (Murata, Ceratron EMS-6081B). The signal from the detector was amplified, discriminated, and processed in electronic circuits based on a microcomputer (NEC, PC-9801RA).

The translational-energy spread of a parent cluster ion was measured to be less than 3 eV (laboratory frame), by changing a retarding potential of the collision region in the fourth OPIG. This energy spread gave rise to the collision-energy spread of 0.2 eV in the center-of-mass frame for the collision of Ni_8^+ with a methanol molecule.

The parent cluster ion, Ni_n^+, passed through a region of 400 mm in length filled with helium gas having a pressure of $\approx 10^{-3}$ Torr. The transit time of Ni_{11}^+, for instance, was estimated to be ≈1 ms at the translational energy of 0.5 eV. The kinetics theory of gases gives ≈200 collisions with helium atoms when the collision cross section is obtained from the geometrical cross sections of Ni_{11}^+ and He. This number of collisions (≈200 times) is sufficient to thermalize Ni_{11}^+, on the basis of the fact that Al_n^+ in He gas is reported to be thermalized when Al_{11}^+ collides with He atoms ≈100 times.[19] Hereafter, the temperature of the helium gas is regarded as the internal temperature of Ni_n^+.

3. Results

Figure 2 shows typical mass spectra of ions produced from Ni_n^+ (n = 4, 6, and 8) following collision with a methanol molecule (CH_3OH) in the collision region. In this measurement, the resolution of the quadrupole mass filter was sacrificed to gaining intensity of the product ions, so that, for instance, the $Ni_n^+(CH_3OH)$ peak was not clearly resolved from the $Ni_n^+(CH_xO)$ ($x \leq 3$) peaks. As shown in Figure 2, every mass spectrum has a peak assignable to $Ni_n^+(CH_3OH)$. The mass spectrum of product ions from Ni_4^+ shows a peak assignable to Ni_4O^+, while that from Ni_8^+ shows a peak assignable to Ni_7C^+.

Let us define the branching fraction for a given product ion, p_i, as

$$f_{p_i} = I_{p_i} / \sum_j I_{p_j} \tag{1}$$

where I_{p_i} and $\sum I_{p_j}$ represent the intensity of the product ion, p_i, and the sum of the intensities of all the product ions observed, respectively. Figure 3 shows the branching fractions as a function of the size of the parent cluster ion. The branching fraction for $Ni_n^+(CH_3OH)$ production has local minima at cluster sizes of 4 and 8, while those of Ni_nO^+ and $Ni_{n-1}C^+$ production have maxima at n = 4 and 8, respectively.

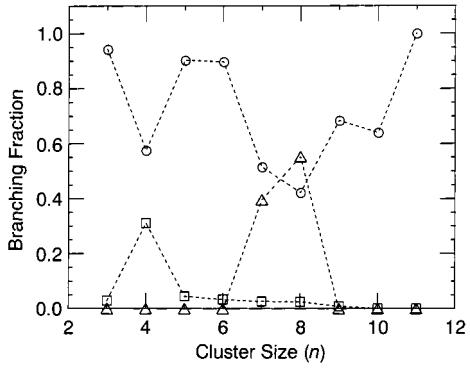

Figure 3. Branching fractions of the product ions as a function of the cluster size: (○) $Ni_n^+ + CH_3OH \rightarrow Ni_n^+(CH_3OH)$, (□) $Ni_n^+ + CH_3OH \rightarrow Ni_nO^+ + CH_4$, and (△) $Ni_n^+ + CH_3OH \rightarrow Ni_{n-1}C^+ + NiO + 2H_2$. The collision energy and the internal temperature are 0.1 eV and 300 K, respectively.

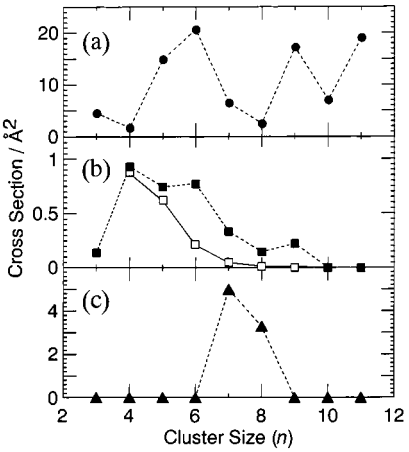

Figure 4. Cross sections for the production of $Ni_n^+(CH_3OH)$ (panel a), Ni_nO^+ (panel b), and $Ni_{n-1}C^+$ (panel c) as a function of the cluster size. The collision energy and the internal temperature are 0.1 eV and 300 K, respectively. The open squares in panel b show the calculated cross sections (see section 4.3).

A total absolute reaction cross section, σ_r, was obtained as

$$\sigma_r = \frac{k_B T}{Pl} \ln \frac{I_r + \sum I_{pi}}{I_r} \tag{2}$$

where I_r represents the intensity of a nonreacting parent ion, P and T are the pressure and the temperature of methanol vapor, respectively, l (=120 mm) is the effective path length of the collision region, and k_B is Boltzmann's constant. A partial absolute reaction cross section, σ_{p_i}, for the formation of a given product ion is given by

$$\sigma_{p_i} = f_{p_i} \sigma_r \tag{3}$$

Figure 4 shows the partial reaction cross sections for the production of $Ni_n^+(CH_3OH)$, Ni_nO^+, and $Ni_{n-1}C^+$ as a function of the cluster size. The cross section for the $Ni_n^+(CH_3OH)$ production reaches local minima at n = 4 and 8, and a global maximum at n = 6 in the size range studied. The cross section for Ni_nO^+ production increases abruptly at n = 4 and then

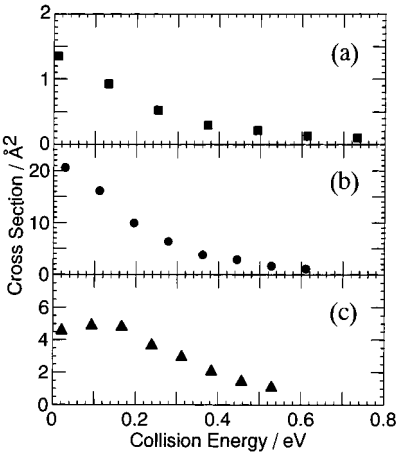

Figure 5. Cross sections for the reactions $Ni_4^+ + CH_3OH \rightarrow Ni_4O^+ + CH_4$ (panel a), $Ni_6^+ + CH_3OH \rightarrow Ni_6^+(CH_3OH)$ (panel b), and $Ni_7^+ + CH_3OH \rightarrow Ni_6C^+ + NiO + 2H_2$ (panel c) as a function of the collision energy. The internal temperature of the parent clusters is 300 K.

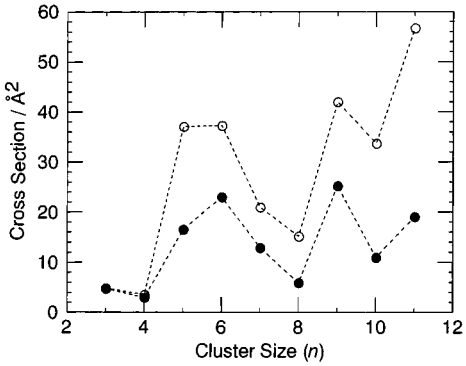

Figure 6. Total reaction cross section as a function of the cluster size. Solid and open circles exhibit the cross sections at the internal temperatures of 300 and 77 K, respectively. The collision energy is fixed at 0.1 eV.

decreases gradually with n, while the cross section for $Ni_{n-1}C^+$ production is sharply peaked at $n \simeq 7-8$ and almost zero otherwise.

Figure 5 shows the partial reaction cross sections as a function of the collision energy. The cross sections for Ni_4O^+ and $Ni_6^+(CH_3OH)$ production from the parent ions, Ni_4^+ and Ni_6^+, respectively, decrease monotonically with the collision energy, as shown in panels a and b, respectively. The monotonic decrease indicates that the reactions for the Ni_4O^+ and the $Ni_6^+(CH_3OH)$ production have no sizable energy threshold within the energy resolution of ± 0.1 eV. A small hump (≈ 0.17 eV) in the collision-energy dependence of the cross section for the production of Ni_6C^+ from Ni_7^+ indicates that this reaction has an energy threshold as low as ≈ 0.1 eV.

Figure 6 shows the total reaction cross section plotted against the size of the parent cluster ion having two different internal temperatures of 77 and 300 K. Both the size dependences at 77 and 300 K exhibit peaks at the same sizes of 6 and 9. The cross sections tend to increase with decreasing the internal temperature; the cross sections at 77 K are about twice as large as those at 300 K.

4. Discussion

4.1. Reaction Scheme. Let us consider a collision event between a methanol molecule, CH_3OH, and a nickel cluster ion, Ni_n^+. Upon CH_3OH approaching Ni_n^+, CH_3OH is at first trapped into a shallow potential well (physisorbed state) due to electrostatic interactions, such as charge−dipole interaction, and then is transferred to a much deeper well (chemisorbed state) attributed to superposition of the electron clouds between CH_3OH and Ni_n^+. It is concluded, therefore, that $Ni_n^+(CH_3OH)$ results from chemisorption of CH_3OH on Ni_n^+. In some cases, the chemisorbed species, $Ni_n^+(CH_3OH)$, further reacts to form Ni_nO^+ or $Ni_{n-1}C^+$ (see Figure 7). All the reaction pathways are given as

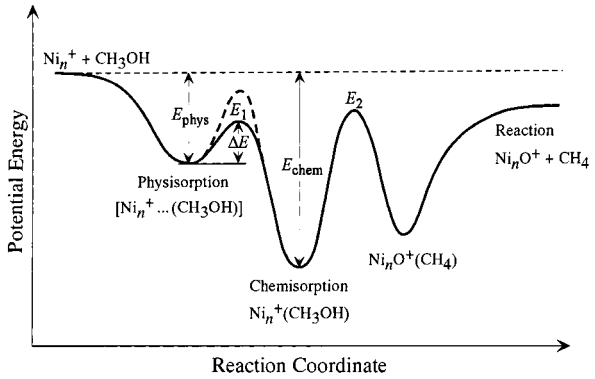

Figure 7. Schematic potential energy surface, which illustrates physisorption, chemisorption, and the demethanation of CH_3OH on Ni_n^+, where E_1 and E_2 represent the potential energies at the transition states.

$$Ni_n^+ + CH_3OH \rightarrow Ni_n^+(CH_3OH) \quad \text{(chemisorption)} \quad (4)$$

$$Ni_n^+ + CH_3OH \rightarrow Ni_nO^+ + CH_4 \quad \text{(demethanation)} \quad (5)$$

$$Ni_n^+ + CH_3OH \rightarrow Ni_{n-1}C^+ + NiO + 2H_2 \quad \text{(carbide formation)} \quad (6)$$

In these reaction processes, the neutral products are not identifiable, because only ionic species are detected in the present experiment. Hence, the most stable and plausible exit reaction channels are exhibited. In the chemisorption process, CH_3OH is chemisorbed either intactly or dissociatively on Ni_n^+. The chemisorbed species can be identified by the comparison with those on a nickel surface as argued in section 4.3. Methanol is likely to be dissociatively chemisorbed on Ni_n^+. In the demethanation process, the formation of CH_4 is the product channel having the lowest energy. In the carbide formation process, on the other hand, NiO should be a major neutral product, because the reaction proceeds via a chemisorbed CH_3OH, in which the oxygen atom is bonded to a Ni atom of Ni_n^+, and NiO is readily separated from the parent cluster ion, $Ni_n^+(CH_3OH)$, together with two hydrogen molecules.

In summary, the production of $Ni_n^+(CH_3OH)$, Ni_nO^+, and $Ni_{n-1}C^+$ corresponds to chemisorption, demethanation, and carbide formation. It is unlikely that $Ni_n^+(CH_3OH)$ detected is a physisorbed species, because the bond is too weak to allow the physisorbed species to survive sufficiently long to reach the detector.

4.2. Chemisorption. The cross section for the chemisorption is estimated by assuming that a methanol molecule, CH_3OH, temporarily trapped in the physisorbed state is either desorbed or is transferred into the chemisorbed state by surmounting an energy barrier, ΔE. The cross section for the chemisorption is given from a cross section for the temporary trapping and the rate constants for the desorption and the transfer to the chemisorbed state. The rate constants were evaluated by RRK

theory (kinematic model),[20] which is simpler than RRKM theory and does not necessitate provision of the vibrational frequencies.

The cross section for the physisorption is approximated by the Langevin scheme in which a polarizable projectile is assumed to collide with a charged target. In the present analysis, the correction by a charge-permanent dipole interaction between Ni_n^+ and CH_3OH is disregarded, because there is no established procedure of the correction and even the upper limit of the correction was found to change ΔE by less than the fitting error of 0.3%. The collision cross section, σ_L (Langevin cross section), is given by

$$\sigma_L = \pi\left(\frac{2\alpha}{E_{col}}\right)^{1/2} \tag{7}$$

where α is the polarizability of CH_3OH ($=3.23 \times 10^{-24}$ cm^3)[21] and E_{col} is the collision energy in the center-of-mass frame.[22] For example, σ_L is equal to 95.8 Å at $E_{col} = 0.1$ eV. The collision occurs effectively at an impact parameter, b, which is less than $(\sigma_L/\pi)^{1/2}$. As shown in eq 7, the Langevin cross section is independent of the cluster size and the internal temperature of the parent cluster ion, whereas the experimental cross sections, which are smaller than the Langevin cross section, depend on the cluster size and the temperature. In the framework of the kinematic model, the dependences on the cluster size and the temperature are introduced from the rate constant, k_1, for desorption from the physisorbed state and the rate constant, k_2, for transferring to the chemisorbed state. Then, the total reaction cross section, σ_r, is given as

$$\frac{\sigma_r}{\sigma_L} = \frac{k_2}{k_1 + k_2} + \frac{k_1}{k_1 + k_2}\exp(-(k_1 + k_2)t) \tag{8}$$

In the present experiment, the reaction time, t, given by the flight time from the collision region to the second quadrupole mass filter, turns out to be several hundred microseconds. In the RRK theory, the rate constants k_1 and k_2 are given by

$$k_1 = A_1\left(\frac{E_{in} + E_{col}}{E_{in} + E_{phys} + E_{col}}\right)^{N-1} \tag{9}$$

$$k_2 = A_2\left(\frac{E_{in} + E_{phys} + E_{col} - \Delta E}{E_{in} + E_{phys} + E_{col}}\right)^{N-1} \tag{10}$$

where A_1 is the prefactor obtained from the degeneracy and the vibrational frequency of an internal mode related to the Ni_n^+–CH_3OH bond dissociation, A_2 is the prefactor related to transfer from the physisorbed to the chemisorbed state, E_{in}, E_{phys}, E_{col}, and ΔE are internal energies of the parent cluster ion, the energy of physisorption, the collision energy, and the energy barrier from the physisorbed to the chemisorbed state, respectively, and N is equal to the total number of the vibrational modes of $Ni_n^+(CH_3OH)$ less the internal modes of CH_3OH. It turns out that $N = [3(n + 6) - 6] - [3 \times 6 - 6] = 3n$.

In order to examine how the internal-energy evaluation influences the ΔE value, the internal energy of Ni_n^+ was estimated from the Jarrold and Bower model[23] and the equipartition model. The ΔE value obtained from the Jarrold and Bower model was found to be larger by 2% than that obtained from the equipartition model. Therefore, the equipartition model was employed to evaluate the ΔE value.

Figure 8 shows the total reaction cross section for Ni_4^+ as a function of its internal temperature. The temperature dependence of the cross section was fit to the theoretical dependence given

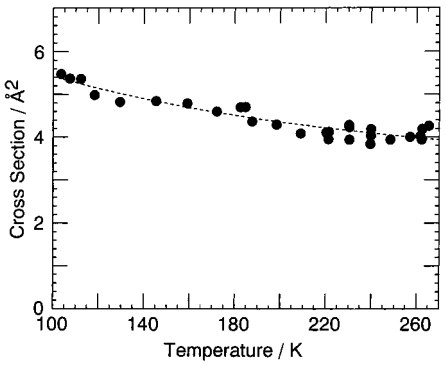

Figure 8. Total reaction cross section for Ni_4^+ as a function of the internal temperature of Ni_4^+. The collision energy is 0.1 eV. The dashed line shows the calculated cross sections with $\Delta E/E_{phys}$ and A_1/A_2 as the best-fit parameters (see text for the definitions); the best-fit values of $\Delta E/E_{phys}$ and A_1/A_2 are 0.96 and 42.8, respectively.

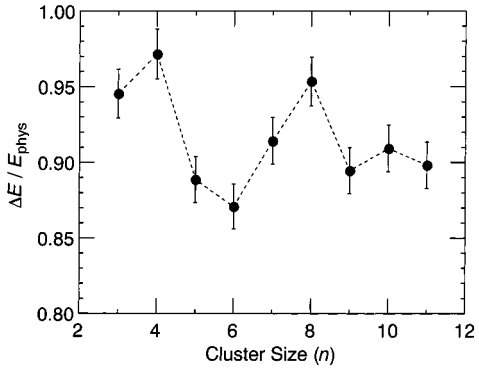

Figure 9. Energy barrier, ΔE, between the physisorbed and the chemisorbed states relative to the physisorption energy, E_{phys}, is plotted against the cluster size. The errors were estimated from the uncertainties in the fitting and the internal-energy evaluation.

by eq 8, leaving $\Delta E/E_{phys}$ as the variable parameter. Figure 9 shows $\Delta E/E_{phys}$ thus obtained as a function of the cluster size. The size dependence of $\Delta E/E_{phys}$ exhibits the global minimum at size 6 and the two maxima at sizes 4 and 8. The size dependence of $\Delta E/E_{phys}$ shows a clear contrast to the size dependence of the reaction selectivity (branching fraction vs size, see Figure 3). Namely, chemisorption is dominant at the size of 6, at which $\Delta E/E_{phys}$ is a minimum, whereas demethanation and carbide formation are dominant at sizes 4 and 8, respectively, at which $\Delta E/E_{phys}$ reaches a maxima. The sharp contrast indicates that (1) chemisorption proceeds more readily when the barrier height is low and (2) demethanation and carbide formation proceed more readily when the barrier height is high.

In $Ni_n^+(CH_3OH)$, CH_3OH may be present as an intact molecular adsorbate, $CH_3OH(a)$, a pair of methoxy and hydrogen adsorbates, $CH_3O(a) + H(a)$, or some other species. A study in ion-stimulated desorption of methanol adsorbed on a nickel(110) surface[24] has revealed that methanol is molecularly adsorbed on the nickel surface below a surface temperature of 140 K, while it is dissociatively adsorbed as $CH_3OH(a) \rightarrow CH_3O(a) + H(a)$ above 240 K. A similar conclusion has been derived from an electron energy loss spectrum of adsorbed methanol on Ni(111):[25] a molecular adsorbate below ≈140 K vs methoxy and hydrogen adsorbates above ≈180 K. These facts imply that CH_3OH in $Ni_n^+(CH_3OH)$ is adsorbed as $CH_3O(a) + H(a)$, because the temperature of $Ni_8^+(CH_3OH)$ rises by ≈200 K as a result of methanol chemisorption, where the energy of the chemisorption is evaluated by assuming that it is equal to the chemisorption energy on an Ni(110) surface, 14 ± 4 kcal/mol.[26] It is possible that CH_3OH is also chemisorbed as CH_3-

(a) + OH(a) by analogy with methanol adsorption on a polycrystalline Ni foil above 140 K.[27]

4.3. Demethanation and Carbide Formation. The demethanation,

$$Ni_n^+ + CH_3OH \rightarrow Ni_nO^+ + CH_4 \qquad (11)$$

is considered to be exothermic as described below. The energetics of the demethanation was obtained by using all the available thermochemical data and the binding energy between Ni_n^+ and O, which was approximated by the binding energies of Cr_n^+-O and V_n^+-O.[28,29] It is then concluded that the demethanation is exothermic by 0.7−3.2 eV in the entire size range studied. It follows that merely size-dependent energetics cannot account for the significant size-dependent reactivities of the demethanation.

As described in section 4.2, the barrier height, $\Delta E/E_{phys}$, has a strong correlation with the cross sections for demethanation and carbide formation, that is, the cross section for demethanation is highest at a size of 4 and that for carbide formation is highest at a size of 8, where the barrier height reaches maxima. Let us consider a schematic reaction potential along the reaction coordinate for physisorption, chemisorption, and demethanation (see Figure 7). There are three valleys corresponding to the physisorbed, the chemisorbed, and the dissociatively chemisorbed states. Two peaks correspond to the transition states with the energies of E_1 and E_2, which were measured relative to the initial state, $Ni_n^+ + CH_3OH$. In the calculation of the demethanation cross section, the energy of the physisorbed state, E_{phys}, is approximated to be 0.4 eV by the energy of a charge-induced dipole interaction, while the energy of the chemisorbed state, E_{chem}, is calculated to be 1.5 eV by using a density functional theory.[30] Throughout the calculation, E_2, E_{phys}, and E_{chem} of CH_3OH to Ni_n^+ are assumed to be independent of n. On the assumption that only the potential energy, E_1 ($=\Delta E - E_{phys}$), changes with the cluster size, the demethanation cross sections were calculated by using the potential energy surface on the basis of the kinematic model (see Figure 7). The relative cross sections for the demethanation thus calculated reproduce the size-dependency of the measured cross sections in the $n \geq 4$ range (see Figure 4). This agreement supports a mechanism that the size-dependent demethanation cross section is controlled by the barrier height, ΔE. The size dependences of the chemisorption energy and the energy of the transition state, E_2, should be taken into account to obtain a reliable size-dependence of the demethanation cross section. The cross section at size 3 does not agree with the measured one, probably for this reason.

The carbide formation,

$$Ni_n^+ + CH_3OH \rightarrow Ni_{n-1}C^+ + NiO + 2H_2 \qquad (12)$$

has a significant cross section only for $n = 7$ and 8. As described above, the barrier height reaches the other maximum at $n = 8$ (see Figure 9). The relation between the cross section and the barrier height seems to be explained similarly by the reaction scheme mentioned in the demethanation. However, this scheme cannot explain the result that the carbide formation proceeds at sizes 7 and 8 but not at size 4, at which the barrier height is high. This difficulty can be solved by introducing a geometrical constraint to a reaction site on Ni_n^+, as is the case of methanol adsorption on a nickel surface, at which surface morphology plays an important role. Upon adsorption of methanol on a nickel surface, a carbon adsorbate, C(a), is produced by the bond rupture of a chemisorbed carbon monoxide, CO(a), supplied from a chemisorbed methanol (or methoxy). The rate of the CO(a) formation depends critically on the surface morphology; for instance, a much larger rate on Ni(111) than on Ni(110).[24−26] The bond rupture of CO(a) is also likely to be morphology-dependent, because CO(a) should occupy two nickel sites in the transition state. By analogy to the surface reaction, one can explain the size-specific reactivity of methanol on Ni_n^+ in terms of matching of the Ni−Ni distance with the C−O distance. In carbide formation, the reaction system ($Ni_n^+ + CH_3OH$) passes through a transition state, in which CH_3OH occupies one nickel atom for its carbon atom and another nickel atom for its oxygen atom. The energy barrier leading to the carbide formation pathway is lowered when the Ni−Ni distance of Ni_n^+ is the most comfortable to CH_3OH in the transition state, that is, the rate of the carbide formation changes sensitively with the Ni−Ni distance. To examine how the Ni−Ni distance of Ni_n^+ changes with n, the Ni−Ni distance was calculated by using density functional methods,[30] and it was found that the distance is elongated at size ≈6 with increase in n as shown in Figure 10. The comparison of this finding with the size-specific reactivity of Ni_n^+ leads us to conclude that the interatomic distance of Ni_n^+ with $n \geq 6$ matches well with the CO bond length of CH_3OH in the transition state, whereas Ni_n^+ with $n < 6$ does not, so that the carbide formation proceeds only on $Ni_{7,8}^+$ but not on Ni_4^+.

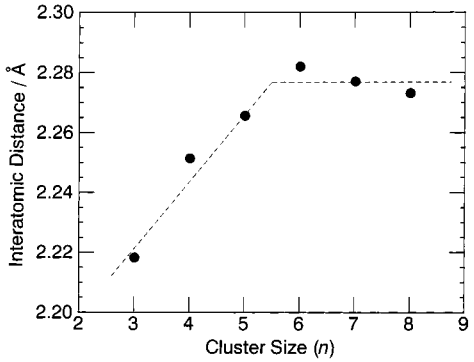

Figure 10. Nearest interatomic distances of Ni_n^+ calculated by a density functional method.[30]

On the other hand, the rate of demethanation does not seem to be sensitive to the Ni−Ni distance because CH_3OH in the transition state responsible for the demethanation occupies a single site on Ni_n^+. Therefore, the demethanation could take place on Ni_4^+ and $Ni_{7,8}^+$. However, the demethanation does not proceed on $Ni_{7,8}^+$, probably because the Ni sites on Ni_n^+ with $n \geq 6$ are occupied more favorably by CH_3OH in the transition state which leads to the carbide formation.

Acknowledgment. We are grateful to Prof. L. H. Wöste and Prof. T. Leisner for advice on the design of the metal ion source employed in the present experiment. Thanks are also due to Prof. S. Tanemura and Dr. J. Murakami for advice on the operation of the metal ion source. This work is supported by Special Cluster Research Project of Genesis Research Institute, Inc.

References and Notes

(1) Irion, M. P.; Selinger, A. *Ber. Bunsen-Ges. Phys. Chem.* **1989**, *93*, 1408.

(2) Irion, M. P.; Schnabel, P.; Selinger, A. *Ber. Bunsen-Ges. Phys. Chem.* **1990**, *94*, 1291.

(3) Irion, M. P. *Int. J. Mass Spectrom. Ion Proc.* **1992**, *121*, 1.

(4) Fayet, P.; McGlinchey, M. J.; Wöste, L. H. *J. Am. Chem. Soc.* **1987**, *109*, 1733.

(5) Vajda, S.; Wolf, S.; Leisner, T.; Busolt, U.; Wö ste, L. H. *J. Chem. Phys.* **1997**, *107*, 3492.

(6) Parks, E. K.; Zhu, L.; Ho, J.; Riley, S. J. *J. Chem. Phys.* **1994**, *100*, 7206.

(7) Zakin, M. R.; Brickman, R. O.; Cox, D. M.; Reichmann, K. C.; Trevor, D. J.; Kaldor, A. *J. Chem. Phys.* **1986**, *85*, 1198.

(8) Knickelbein, M. B. *Chem. Phys. Lett*. **1995**, *239*, 11.

(9) Knickelbein, M. B. *J. Chem. Phys.* **1996**, *104*, 3517.

(10) Knickelbein, M. B.; Koretsky, G. M. *J. Phys. Chem*. **1998**, *102*, 580.

(11) Dietrich, G.; Dasgupta, K.; Krückeberg, S.; Lützenkirchen, K.; Schweikhart, L.; Walther, C.; Ziegler, J. *Chem. Phys. Lett.* **1996**, *259*, 397.

(12) Rousseau, R.; Dietrich, G.; Krückeberg, S.; Lützenkirchen, K.; Marx, D.; Schweikhart, L.; Walther, C. *Chem. Phys. Lett.* **1998**, *295*, 41.

(13) Dietrich, G.; Krückeberg, S.; Lützenkirchen, K.; Schweikhard, L.; Walther, C. *J. Chem. Phys.* **2000**, *112*, 752.

(14) Rousseau, R.; Marx, D. *J. Chem. Phys.* **2000**, *112*, 761.

(15) Ichihashi, M.; Hirokawa, J.; Nonose, S.; Nagata, T.; Kondow, T. *Chem. Phys. Lett.* **1993**, *204*, 219.

(16) Ichihashi, M.; Nonose, S.; Nagata, T.; Kondow, T. *J. Chem. Phys.* **1994**, *100*, 6458.

(17) Hirokawa, J.; Ichihashi, M.; Nonose, S.; Tahara, T.; Nagata, T.; Kondow, T. *J. Chem. Phys.* **1994**, *101*, 6625.

(18) Ichihashi, M.; Yadav R. T.; Kondow, T. In *Physics and Chemistry of Clusters*; Springer: Heidelberg, in press.

(19) Ingólfsson, O.; Takeo, H.; Nonose, S. *J. Chem. Phys.* **1999**, *110*, 4382.

(20) Draves, J. A.; Luthey-Schulten, Z.; Liu, W.-W.; Lisy, J. M. *J. Chem. Phys.* **1990**, *93*, 4589.

(21) Hirschfelder, J. O.; Curtiss, C. F.; Bird, R. B. *Molecular Theory of Gases and Liquids*; John Wiley & Sons: New York, 1963.

(22) Levine, R. D.; Bernstein, R. B. *Molecular Reaction Dynamics*; Oxford University Press: Oxford, 1974.

(23) Jarrold, M. F.; Bower, J. E. *J. Chem. Phys.* **1987**, *87*, 5728.

(24) Vajo, J. J.; Campbell, J. H.; Becker, C. H. *J. Phys. Chem.* **1991**, *95*, 9457.

(25) Demuth, J. E.; Ibach, H. *Chem. Phys. Lett.* **1979**, *60*, 395.

(26) Richter, L. J.; Ho, W. *J. Chem. Phys.* **1985**, *83*, 2569.

(27) Steinbach, F.; Krall, R.; Cai, J.-X.; Kiss, J. In *Proceedings of the 8th Internernational Congress on Catalysis*; Berlin, July, 1984; Verlag Chemie: Weinheim, 1984; Vol. 3, p III-359.

(28) Griffin, J. B.; Armentrout, P. B. *J. Chem. Phys.* **1998**, *108*, 8062.

(29) Xu, J.; Rodgers, M. T.; Griffin, J. B.; Armentrout, P. B. *J. Chem. Phys.* **1998**, *108*, 9339.

(30) Yadav, R. T.; Hanmura, T.; Ichihashi, M.; Kondow, T., unpublished data.